JOURNAL OF THERMOPHYSICS AND HEAT TRANSFER
Vol. 6, No. 2, April–June 1992

Earth Atmospheric Entry Studies for Manned Mars Missions

M. E. Tauber* and G. E. Palmer†
NASA Ames Research Center, Moffett Field, California 94035
and
Lily Yang‡
Sterling Software, Palo Alto, California 94303

The lift/drag ratios (*L/D*s) required, and the decelerations, heating rates, and total heat loads encountered when returning from Mars to Earth at entry speeds of 12 km/s to 16 km/s are studied. An entry velocity of 14 km/s is emphasized because it is the fastest entry presently envisioned for manned missions. For entry at 14 km/s, it is found that an *L/D* of 0.5 is required to provide a guidance corridor margin near 1 deg for the specified deceleration limit of 5 *g*. The *L/D* of 0.3 of the Apollo shape is found to be inadequate. The stagnation point peak heating rates range from about 0.87 kW/cm² for the overshoot trajectory to 1.33 kW/cm² at undershoot, for a ballistic coefficient of 300 kg/m². For a blunted, raked cone with an *L/D* = 0.5, the peak heating rate near the aft end of the forebody varies from 0.14 to 0.23 kW/cm² for laminar flow; but if ablation triggers boundary-layer transition, the peak heating can rise to 0.5 or up to 0.72 kW/cm². All heating rates are sufficiently high to make ablative heat shields necessary. The stagnation point total heat load is about 100 kJ/cm². The total heat loads near the aft end of the forebody are about 20 kJ/cm² for a laminar boundary layer; the heat load approches 90 kJ/cm² if fully turbulent flow is assumed during the entire entry.

Nomenclature

A = reference area of entry vehicle, m²
C_D = drag coefficient
C_L = lift coefficient
D = drag
L = lift
m = vehicle mass, kg
r_n = vehicle nose radius, m
V = flight velocity
x = distance along body surface
α = angle of attack
γ = flightpath angle
θ_c = body half-angle
ρ = freestream density, kg/m³

Subscripts
E = entry condition
e = boundary-layer edge
w = vehicle wall

Introduction

A NUMBER of studies conducted during the past 25 years have shown that using atmospheric braking at both Earth and Mars during manned missions to Mars can reduce the weight that must be placed in low Earth orbit by 50% to 75%.[1–4] Early missions will be the short, opposition type that last only 14 to 17 months,[5,6] to maximize the safety of the crew. By necessity, these shorter missions will result in higher entry velocities at Mars and on return to Earth.

The objectives of this study are to investigate the *L/D*s required, the decelerations experienced by the crew, and the heating of the vehicle during atmospheric entry on return to Earth. For the missions under consideration, the entry speeds can vary from as high as 16 km/s to less than 12 km/s.[5,6] The large variation of entry velocities stems from many factors, including the departure date (which determines the relative position of Earth and Mars), total trip duration, and use of a Venus swingby maneuver to reduce the arrival speed at Earth.[7] However, it should be kept in mind that the reduction in entry velocity afforded by Venus swingbys usually increases mission time and always exposes the crew to much greater radiation hazards from potential solar flares. In fact, short trip times may be required to lessen the exposure to both solar and cosmic radiation.[8] In addition, the vehicle must be shielded from solar heating. For example, a Venus swingby on the Mars-bound leg may require extensive solar heat shielding to reduce boil-off of cryogenic propellants.

During NASA's Apollo lunar exploration program, unique experience was gained with manned vehicles that entered the Earth's atmosphere at the parabolic speed of 11 km/s. When returning to Earth from planetary missions, entries occur at hyperbolic speeds; as previously mentioned, velocities up to 16 km/s will be considered. Hyperbolic speed entries can be performed directly in a single pass, or by making multiple atmospheric passes. However, the first aerobraking pass must always decelerate the vehicle to below parabolic speed to ensure planetary capture. Although multiple-pass braking maneuvers can be performed, it was shown long ago[9,10] that more precise guidance is required and that the total heat input is greater than for a single pass entry. Therefore, only single pass, direct entries are considered here. It is also assumed that the vehicle decelerates enough to permit a safe (parachute-assisted) landing.

The vehicle configurations considered are limited to capsule-like shapes. Heating rates at hyperbolic speeds become very large, as will be shown, and ablative heat shields are mandatory. Therefore, capsule-like configurations that have small windward surface areas are required. In contrast, the large windward surfaces of winged vehicles would result in large heat shield mass fractions.

The paper begins with a definition of the major parameters and the vehicle configurations to be studied. A brief descrip-

Presented as Paper 90-1699 at the AIAA/ASME 5th Joint Thermophysics and Heat Transfer Conference, Seattle, WA, June 18–20, 1990; received Sept. 18, 1990; revision received Feb. 12, 1991; accepted for publication March 8, 1991.

*Research Scientist. Associate Fellow AIAA.
†Research Scientist. Member AIAA.
‡Research Specialist.

tion of the analysis technique follows. The final results consist of trajectories, deceleration pulses, flowfields, heating rates, and total heat loads at key body locations.

Study Parameters

The present study concentrates on direct entries into Earth's atmosphere of a capsule-like vehicle carrying only four to six occupants and a limited amount of surface material from Mars. In some recent studies, it has been somewhat arbitrarily stipulated that the Earth entry velocity be kept at, or below, 12.5 km/s for normal missions[6] with an upper limit of 14 km/s if a mission has to be aborted. Because the vehicle must be designed for the 14 km/s entry condition, this speed is emphasized throughout the study. However, key results will also be shown for a broader range of entry speeds varying from about 12 to 16 km/s.

Because the welfare of the crew is a primary concern, NASA has tentatively limited the total deceleration load experienced by the crew to 5 g because of the debilitating effect on the crew of the long mission. Therefore, the guidance precision required will be more stringent than that for the Apollo lunar return entries, which had a 10-g limit. However, guidance capability for the Mars mission should be greatly improved in comparison with the Apollo mission. Onboard computational capabilities will likely have advanced by several orders of magnitude and can be supplemented by ground- and satellite-based navigational aids.

Configurations having L/Ds ranging from 0.2 to 0.5 are considered. The configuration having an L/D of 0.5 at α = 0 deg consists of a blunt-nosed, raked cone with a slightly elliptical cross section (eccentricity of 1.235) forebody. This forebody shape offers good lateral and longitudinal stability and has its maximum lift coefficient and peak L/D near zero angle of attack. Therefore, attitude control is simplified because maximum C_L is used at the overshoot, and maximum L/D at the undershoot, boundaries. Furthermore, the absence of crossflow at α = 0 deg delays boundary-layer transition, which reduces heating. In addition, the Apollo shape, having an L/D of 0.3 at α = 25 deg, is considered. Although the Apollo can develop somewhat greater L/Ds at higher angles of attack, the afterbody would be exposed to high heating, thus greatly increasing the heat shielding weight. For the low L/D shape, a blunted 70 deg half-angle cone is used. This configuration has an L/D = 0.2 at α = 14 deg. Sketches of all configurations are shown in Fig. 1. Ballistic coefficients (m/C_DA) of 300 and 500 kg/m^2 are considered, with the former being used as a primary value. For comparison, the Apollo had a value of about 340 kg/m^2; however, its heat shield was grossly overdesigned and the structure was designed for at least 10 g, or twice the load factor of the Mars return entry capsule.

The radiative and convective heating rates are calculated at the stagnation point and at the bottom forebody centerline, just ahead of the corner, where the maximum boundary-layer edge Reynolds number occurs. Laminar, transitional, and turbulent boundary-layer heating is considered off the stagnation point. The surface pressures are assumed to be sufficiently large during the high-heating portion of the entry so that nonequilibrium radiative processes could be neglected. The total, time-integrated heat loads are also shown. Only the heating rates occurring in the absence of ablation are calculated and shown. The results presented are, therefore, independent of the heat shield material and can be used to study a variety of candidate materials.

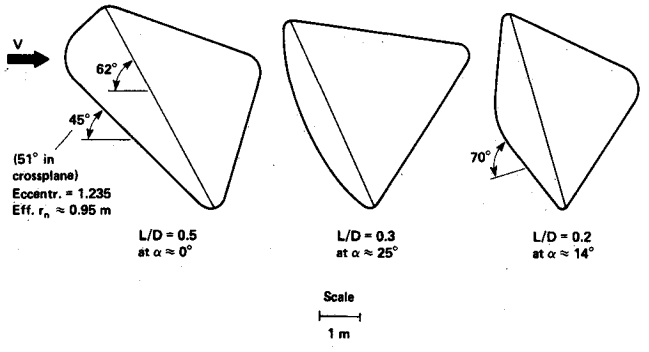

Fig. 1 Entry configurations studied.

Analysis

The trajectory equations for a nonrotating planet are employed to calculate flight paths along a great circle route. The 1962 U.S. Standard Atmosphere model is used. The laminar stagnation point heat transfer rates are based on the relations given in Ref. 11. The laminar, transitional, and turbulent heating relations used on the conical surface, beyond the influence of the blunt nose, are given in Ref. 12. The turbulent convective heating relations were derived using the reference enthalpy procedure.[13] Fully catalytic surfaces have been assumed because ablative heat shielding is required, as will be shown. Many ablators form carbon char surfaces that are highly reactive but reradiate a significant fraction of the incoming heat. The equilibrium radiative heating at the stagnation point is based on nonadiabatic flow calculations that have been correlated in Ref. 14 and listed in the appendix, also. The calculations take into account self-absorption over the entire spectrum and have been extensively compared with experimental measurements.[15]

Flowfields about the vehicle are computed numerically for several representative flight conditions. A time-dependent method is used to solve the Navier-Stokes equations for weakly ionized viscous flow about the forebody.[16] Thermodynamic equilibrium is assumed, but finite chemical reaction rates are used for 11 constituent species. Boundary-layer transition is modeled using a correlation of boundary-layer edge values of Reynolds number and Mach number for walls having $T_w \ll T_e$. The validity of the above correlation parameters is supported by a recent study of supersonic boundary-layer stability for nonablating bodies.[17]

The radiation on the conical surface, beyond the influence of the blunt-nose produced high entropy gas layer, is calculated one-dimensionally using the velocity component normal to the shock wave. The radiative and convective heating are assumed to be uncoupled in the calculations. This assumption is valid if the radiative heating is much less than the total flow energy ($1/2\rho V^3$) and is applicable for all flight conditions considered here. Assuming that the radiation and convection are uncoupled implies that the boundary-layer edge temperature is only slightly reduced by radiative cooling; this assumption is plausible because the shock-layer radiative emission is a highly nonlinear function of temperature.

Results

The presentation begins with a discussion of entry trajectories and the L/Ds that are required. The deceleration pulses and peak g-loads are shown next. This is followed by some examples of the computed flowfield properties. The heating environment encountered by the vehicle during entry is shown last. Nonablating-wall heating pulses, peak heating rates, and total heat loads at two body locations are presented.

Atmospheric Trajectories

Trajectories are computed for flight conditions near, or at, the undershoot and overshoot boundaries. The undershoot trajectories are constrained by the 5-g deceleration limit. The overshoot case is determined by the maximum lift that is available to prevent atmospheric skip-out at hyperbolic speeds. The difference between the overshoot and undershoot boundaries is the corridor width, which can be measured in terms of the altitude difference, entry flight-path angles or peak decelerations. The last case is illustrated in Fig. 2, which shows the peak g-load near overshoot as a function of entry speed

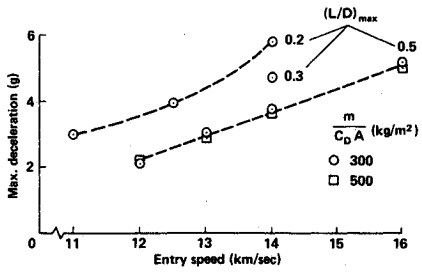

Fig. 2 Peak total decelerations during shallow Earth entry.

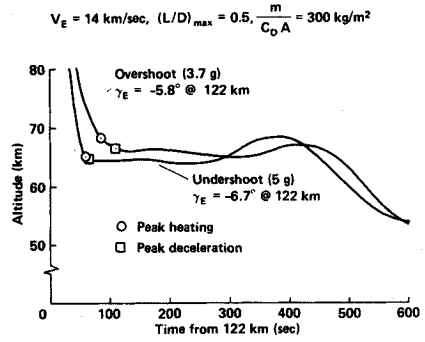

Fig. 3 Earth direct entry trajectories.

for maximum L/D values of 0.2, 0.3, and 0.5. (Lines are drawn through the 0.2 and 0.5 values.) Ballistic coefficients of 300 and 500 kg/m² are used; however, the peak deceleration is nearly independent of this parameter. Note that the corridor becomes extremely narrow (0.3 g) for $L/D = 0.3$ (the Apollo shape) at a 14 km/s entry speed. For a 16 km/s entry the L/D must be greater than 0.5 if the corridor width is to be finite.

To provide a reasonable guidance and control margin, most of the example entries considered here will be for $L/D = 0.5$. The overshoot and undershoot trajectories for the nominal 14 km/s entry and a ballistic coefficient of 300 kg/m² are shown in Fig. 3. The flight-path angle margin is about 0.9 deg at the 122 km altitude where entry is defined to begin. The times for peak heating and maximum deceleration are labeled and occur early, at high speeds, as is to be expected. Lift modulation was used to calculate these and all other trajectories. However, the terminal part of the entry, starting at 4 km/s, is a constant L/D glide path. (Our colleague J. E. Lyne recently began to refine the control algorithm that was used in this paper to modulate the L/D. His initial results indicate that the entry angle corridor can be made somewhat larger than the values shown here. The values presented in this paper are, therefore, conservative. However, the deceleration and heating pulses to be shown and the conclusions drawn here should not be significantly affected.)

Deceleration Pulses

As seen in Fig. 3, much of the deceleration occurs at nearly constant altitudes in the vicinity of 65 km. In fact, the vehicle slows to half its entry speed within the first 4 to 5 min. In addition to the peak g-load experienced by the crew, the duration of the deceleration pulse is also physiologically important. Overshoot and undershoot deceleration pulses are shown in Fig. 4 for trajectories with peak $L/D = 0.5$ and bodies with ballistic coefficients of 300 and 500 kg/m² entering at 14 km/s. (As already noted in Fig. 2, the peak g-load at overshoot is insensitive to ballistic coefficient.) The crew experiences more than 2 g for only about 3 min; this duration should not be hazardous for reasonably physically fit individuals.

The deceleration pulse for the Apollo configuration having an $L/D = 0.3$ is shown in Fig. 5. This pulse is also calculated near the overshoot boundary. However, the peak deceleration of 4.7 g that occurs is only 6% below the 5-g undershoot

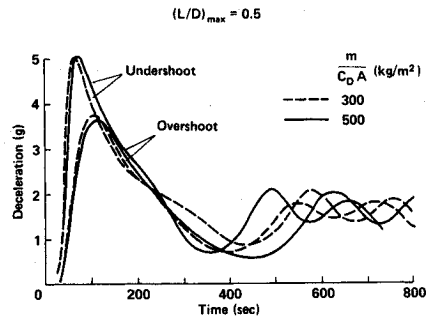

Fig. 4 Total deceleration history during Earth entry at 14 km/s.

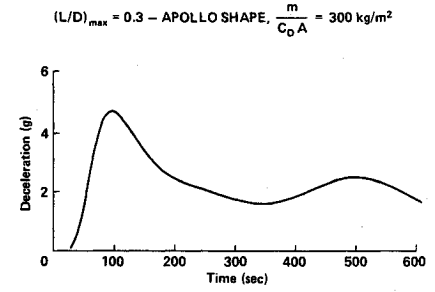

Fig. 5 Total deceleration history during Earth entry at 14 km/s.

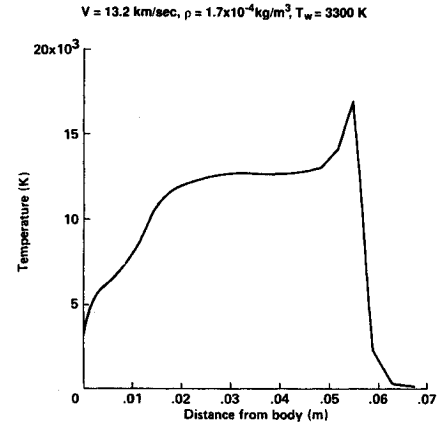

Fig. 6 Shock-layer temperature distribution–stagnation line.

limit. Thus, the deceleration pulse at the undershoot boundary should be very similar. During the initial deceleration, the crew is subjected to more than 2 g for 3.5 min, although a second pulse reaches 2.5 g about 500 s after entry.

Flowfields

The flow about the $L/D = 0.5$ configuration has been calculated for several entry speeds near peak heating. To simplify the modeling and to reduce the computation time, an axisymmetric forebody shape (circular cross section, or eccentricity of one) is assumed. Results will be shown for the stagnation line and for one body location in the vertical plane of symmetry. The flow at these locations should be essentially unaffected by the assumption of axial symmetry. A 49 × 49 grid is used, and about 12,000 time steps are required for convergence. A well-converged solution takes about 35 min of CPU time on a Cray 2 computer. Representative results will be shown for a velocity of 13.2 km/s and a free-stream density of 1.7×10^{-4} kg/m³. This flight condition is close to the undershoot boundary and near where peak heating occurs (see Fig. 3). A fully catalytic wall at a temperature of 3300 K has been assumed on the forebody in the computation; this temperature is representative of several types of ablators such as AVCOAT and phenolic nylon.

The temperature variation along the stagnation streamline is shown in Fig. 6. Note that the only region where chemical

reactions influence the flow strongly is right behind the shock for a distance of about 15% of the shock layer thickness. The finite rate of the chemical reactions causes the temperature to rise to about 17,000 K just aft of the shock; downstream the temperature stabilizes at a value of about 12,500 K as the atomic nitrogen and oxygen ionize (see Fig. 7). Although atoms still dominate the mixture, ionized species approach 25% of the mole fraction as shown in Fig. 7. (Obviously, the calculated level of the ionization violates the assumption of weak ionization that is used in the formulation of the energy equation. However, the Debye length, which is a measure of the distance over which Coulomb forces from charged particles act, is six orders of magnitude less than the shock standoff distance. Also, because thermodynamic equilibrium is assumed, the electron and heavy particle temperatures are the same. Therefore, the present formulation should not result in large errors at the flight conditions near peak heating.)

The shock-layer temperature and composition profiles are also presented at the cone forebody bottom centerline in Figs. 8 and 9, respectively. As expected, the temperature in much

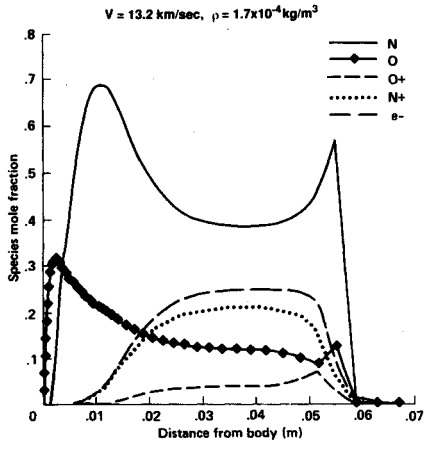

Fig. 7 Species distribution–stagnation line.

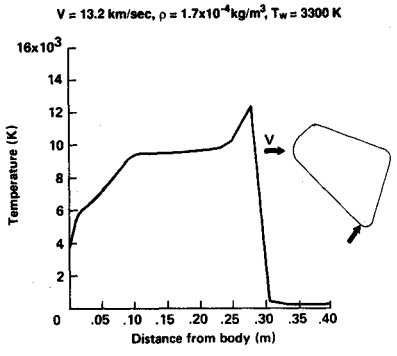

Fig. 8 Shock-layer temperature distribution–bottom centerline.

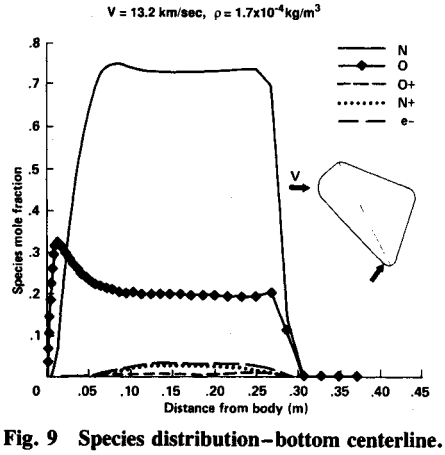

Fig. 9 Species distribution–bottom centerline.

of the shock layer is about 3000 K lower than along the stagnation streamline. Therefore, the mole fraction of ions is only about 3% at this body location. Again, most of the chemical nonequilibrium effects occur in the first 15% of the shock layer. Therefore, the assumption that the shock layer is in chemical equilibrium should be reasonably good when computing radiative heating for the flight conditions considered here. The 10% increase in the temperature near the wall is probably caused by a remnant of the high-entropy gas that has passed through the blunt nose shock.

Heating Rates

The stagnation point peak heating rates are shown as a function of nose radius in Fig. 10 for trajectories with maximum L/Ds of 0.2 and 0.5 and an entry speed of 14 km/s. (The difference between the total heating rate and the equilibrium radiation is the convective heating.) The heating values are calculated for the overshoot trajectory with $L/D = 0.5$. The $L/D = 0.2$ case is presented for comparison only because the 5-g limit is exceeded, as shown in Fig. 2. For the $L/D = 0.5$ configuration, which has a slightly elliptical forebody (Fig. 1), an effective nose radius of 1 m is used, although the actual value is closer to 0.95 m. The heating rate approaches a minimum near a nose radius of 1 m and is insensitive to small deviations from this value. (Convective heating becomes large for smaller nose radii.) As the nose radius is increased to 2 m, the radiation becomes more intense, but the combined heating rate rises by only 5% and the total heat load during the entry decreases by 3.5%. However, the nose radius cannot be arbitrarily increased without decreasing the L/D. This fact has been ignored in calculating the heating rates shown in Fig. 10. When the L/D decreases to 0.2, the peak heating rates increase by about 45%. Note that most of the heating is caused by (equilibrium) radiation; the rationale for assuming equilibrium is supported by the fact that the peak stagnation pressures are in the vicinity of 0.3 atm, or greater.

The stagnation point heating pulses for the overshoot and undershoot trajectories are shown in Fig. 11 for a 1-m nose radius. The peak heating rate at undershoot is about 54% higher than at overshoot; however the total heat loads are nearly the same, as will be shown later. Note that the radiative heating pulses are more intense than the convective pulses, but the former last only about half as long.

On the conical surface beyond the influence of the vorticity layer from the blunt nose, the radiative heating becomes small; but if boundary-layer transition occurs, turbulent convection can be severe. In Fig. 12, the heating for the undershoot and overshoot trajectories is shown at a point near the end of the cone forebody along the bottom centerline. If the surface roughness from ablation remains small compared to the boundary-layer thickness in the critial nose region, a laminar boundary layer may be maintained[18] because the maximum

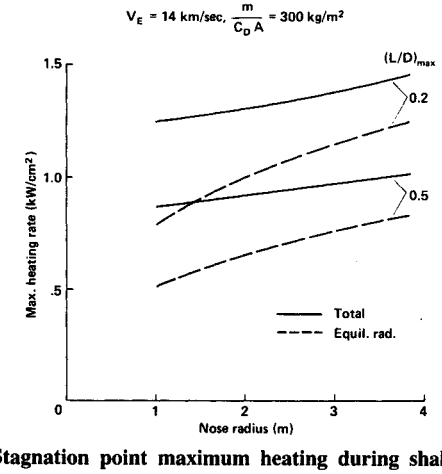

Fig. 10 Stagnation point maximum heating during shallow Earth entry.

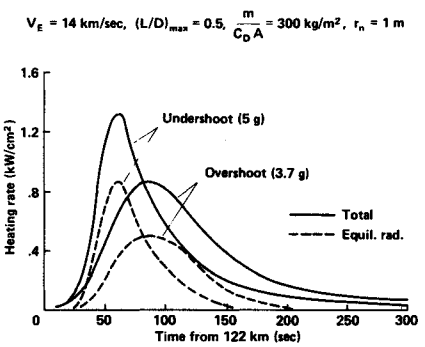

Fig. 11 Stagnation point heating rates for Earth entry.

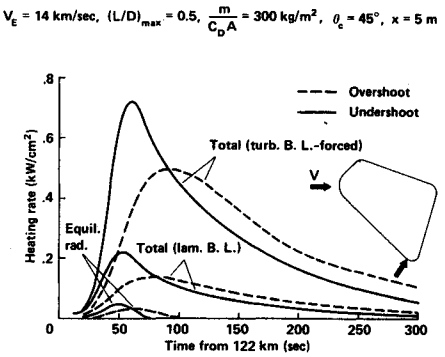

Fig. 12 Heating rates on centerline near end of cone forebody during Earth entry.

boundary-layer edge Reynolds number at this body location is only 8×10^5 for a ballistic coefficient of 300 kg/m², and 1.6×10^6 for 500 kg/m². Another factor that can cause transition is mass addition from ablation. If the ratio of mass addition to boundary-layer edge mass flow can be kept small by using materials with high intrinsic heats of ablation, then laminar flow may be maintained to local Reynolds numbers of about 4 million.[19] The local Mach number of about 3.5 at this body location is nearly the same as in the ballistic range experiments of Ref. 19. In wind tunnel experiments,[20] mass addition has been observed to trigger transition on blunt bodies (where Mach numbers are subsonic or transonic) when Reynolds numbers based on nose diameter exceeded one million. However, for the present flight case, the comparable nose-Reynolds numbers are an order of magnitude lower and the boundary layer may well be laminar. In that case, as shown in Fig. 12, the peak heating rate is only 0.22 kW/cm². However, if the very conservative assumption is made that transition is triggered near the sonic line on the nose, the peak heating rates are at least tripled (Fig. 12).

Apollo-shaped vehicles are frequently considered for future manned atmospheric entries because of the experience gained with that configuration during the lunar exploration missions. At the lunar return entry speed of 11 km/s, convection is the dominant heating mechanism and a blunt-faced configuration controls heating effectively. However as the entry speed increases, radiative heating becomes large. At an entry speed of 14 km/s, an Apollo-shaped body experiences 80% of its stagnation point peak heating from shock layer radiation (Fig. 13). Despite the 25-deg angle of attack that was used for the case shown in Fig. 13, at overshoot the stagnation point peak heating rate is 1.25 kW/cm²; this is nearly as high as the blunted, raked cone value of 1.33 kW/cm², which occurs at the undershoot boundary. Not only are the radiative heating rates higher for the Apollo shape, but the low L/D and the resultant severe guidance difficulties make the configuration unsuitable for entry at 14 km/s.

The stagnation point peak heating rates for the blunted, raked cone are shown in Fig. 14 as a function of entry velocity. The calculations are primarily for the overshoot flight con-

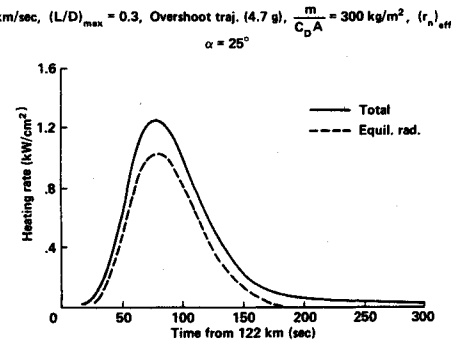

Fig. 13 Stagnation point heating rates for Apollo-shaped Earth entry vehicle.

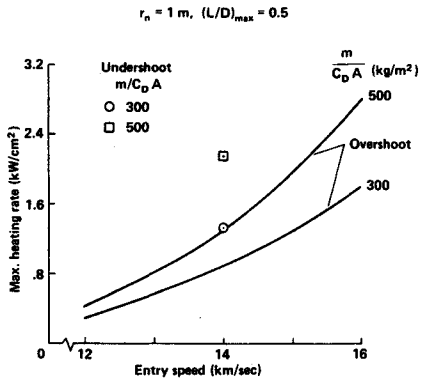

Fig. 14 Maximum stagnation point heating rates during Earth entry. (Lines for overshoot, points for undershoot boundaries.)

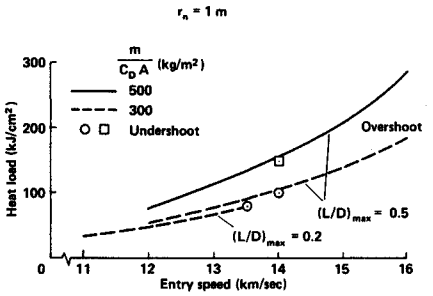

Fig. 15 Total stagnation point heat loads during Earth entry. (Lines for overshoot, points for undershoot boundaries.)

ditions. As expected, the peak heating rate rises with increasing ballistic coefficient; the increase varies from 45% for the 12 km/s entry to 55% for the 16 km/s case. For entry at 12 km/s, the stagnation point peak heating rates are only about 35% of the values experienced at 14 km/s. For the 16 km/s entry, the values are over twice as high as for the 14 km/s case.

Total Heat Loads

The stagnation point total heat loads are presented in Fig. 15 as a function of entry velocity. The calculations are, again, primarily for the overshoot trajectories. At the overshoot boundary, the vehicle usually experiences higher total heat loads than at undershoot, although the differences may become small as can be seen in Fig. 15. The total heat input rises as the ballistic coefficient increases from 300 to 500 kg/m². The increase varies from 45% for a 12 km/s entry to 55% for the 16 km/s case. The heat load also doubles as the entry speed increases from 12 to 14 km/s. The stagnation point heat load is much more sensitive to ballistic coefficient than to L/D. Note that the heat loads for the trajectories having a peak L/D of 0.5 are only about 15% higher than for the L/D = 0.2 cases. The stagnation point total heat load of the Apollo configuration (L/D = 0.3) is 100 kJ/cm² and corre-

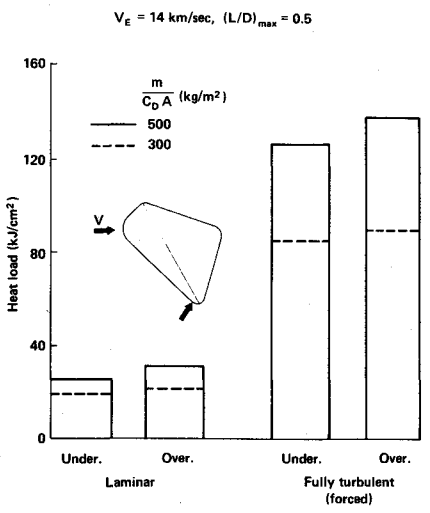

Fig. 16 Total heat loads on centerline near end of cone forebody during Earth entry.

sponds to the heating pulse shown in Fig. 13. For entry at 14 km/s, the Apollo configuration has nearly the same stagnation point heat load as the $L/D = 0.5$ case shown in Fig. 15.

The heat loads near the end of the conical forebody for the raked cone's centerline are shown in Fig. 16; the entry speed is 14 km/s. The values shown in Fig. 16 represent the time-integrated heating rates for the pulses illustrated in Fig. 12. The differences in heat loads for the undershoot and overshoot trajectories range from 5% to 13% at this body location. Most noticeable in Fig. 16 is the approximately four-fold increase in heat load if the boundary layer is assumed to be fully turbulent during the entire entry. This very conservative assumption of boundary layer transition results in heat loads that are only about 10% less than the corresponding stagnation point values that are shown in Fig. 15.

Concluding Remarks

Decelerations, heating rates, and total heat loads encountered are studied at Earth atmospheric entry speeds of 12 to 16 km/s. An entry velocity of 14 km/s has been emphasized. The 14 km/s case is the fastest entry presently envisioned for manned return from Mars and would be experienced during an aborted mission. For entry at 14 km/s, it was found that an L/D of 0.5 was required to provide a guidance corridor margin approaching 1 deg for the specified deceleration limit of 5 g. The L/D of 0.3 of the Apollo shape was found to be inadequate. The period during which the deceleration exceeds 2 g lasts about 3 min. The stagnation point peak heating rates varied from about 0.87 kW/cm² for the overshoot trajectory to 1.33 kW/cm² at undershoot, for a ballistic coefficient of 300 kg/m². For a blunted, raked, conical configuration with an $L/D = 0.5$, the peak heating rate near the aft end of the forebody varies from 0.14 to 0.23 kW/cm² for laminar flow. However, if surface roughness from ablation triggers early boundary layer transition, the peak heating near the aft end of the forebody can rise to 0.5 or up to 0.72 kW/cm². All heating rates are sufficiently high to make ablative heat shields necessary. The stagnation point total heat load is about 100 kJ/cm². The total heat loads near the aft end of the forebody are about 20 kJ/cm² for a laminar boundary layer; the heat load approaches 90 kJ/cm² if fully turbulent flow is assumed during the entire entry. Using the same vehicle configuration, but increasing the ballistic coefficients from 300 kg/m² to 500 kg/m², raises the stagnation point peak heating rates and total heat loads by about 50%. At the aft end of the cone forebody, the increase in the ballistic coefficient causes the total heat loads to rise an average of 37% for the laminar flow cases and about 50% for the fully turbulent flow cases.

Table A1 Radiative heating velocity functions for air

V, m/s	$f(V)$	V, m/s	$f(V)$
9,000	1.5	12,000	359
9,250	4.3	12,500	495
9,500	9.7	13,000	660
9,750	19.5	13,500	850
10,000	35	14,000	1,065
10,250	55	14,500	1,313
10,500	81	15,000	1,550
10,750	115	15,500	1,780
11,000	151	16,000	2,040
11,500	238		

Appendix

An expression having the form

$$\dot{q}_r = C r_n^a \rho^b f(V) \tag{A1}$$

is used to represent the equilibrium radiative heating values at the stagnation point in air over a range of flight conditions representative of Mars missions. In Eq. (A1), C is a constant that depends on the atmosphere, r_n is the hemispherical nose radius in m, ρ is the free-stream density in kg/m³, and $f(V)$ are tabulated values that are functions of flight velocities V and the atmospheric composition. The exponent a is a function of ρ and also V, in m/s; the exponent b is a constant. The following values are used, where $\dot{q}_r$ is in W/cm²:

$$C = 4.736 \times 10^4$$

$$a = 1.072 \times 10^6 V^{-1.88} \rho^{-0.325}$$

$$\text{if } 1 \le r_n \le 2, \quad a \le 0.6$$

$$\text{if } 2 < r_n \le 3, \quad a \le 0.5$$

$$b = 1.22 \tag{A2}$$

Values of $f(V)$ are listed in Table A1; linear interpolation can be used. The values given by Eqs. (A1) and (A2) apply in the speed range from 10 km/s to 16 km/s, and for free stream densities from 6.66×10^{-5} kg/m³ to 6.31×10^{-4} kg/m³, or altitudes of about 72 km to 54 km, respectively. The nose radii can vary from 0.3 m to 3 m. (Note that $a \le 1$ must always be met.)

References

[1]Syvertson, C. A., and Dennis, D. H., "Trends in High-Speed Atmospheric Flight," AIAA First Annual Meeting and Technical Display, Washington, DC, July 1964; also NASA TM-X-54,062.

[2]Tauber, M. E., and Seiff, A., "Optimization of Heating of Conical Bodies Making Lifting Hyperbolic Entries into the Atmospheres of Earth and Mars," AIAA Entry Technology Conf., Williamsburg, VA, Oct. 1964.

[3]Clark, B., "Manned Mars Missions for the Year 2000," AIAA Paper 89-0512, Reno, NV, Jan. 1989.

[4]Braun, R. D., and Blersch, D. J., "Propulsive Options for a Manned Mars Transportation System," AIAA Paper 89-2950, Reno, NV, Jan. 1989.

[5]Tauber, M. E., Bowles, J., and Yang, L., "The Use of Atmospheric Braking During Mars Mission," *Journal of Spacecraft and Rockets*, Vol. 27, No. 5, 1990, pp. 514–521.

[6]Braun, R. D., "The Effect of Interplanetary Trajectory Options on a Manned Mars Aerobrake Configuration," NASA TP 3019, Aug. 1990.

[7]Deerwester, J. M., and D'Haem, S. M., "Systematic Comparison of Venus Swingby Mode with Standard Mode of Mars Round Trip," AIAA Paper 67-27, New York, Jan. 1967.

[8]Lawler, A., "Space Radiation Hazard Threatens Mars Mission," *Space News*, Vol. 1, No. 7, 1990, p. 8.

[9]Chapman, D. R., "An Approximate Analytical Method for Studying Entry into Planetary Atmospheres," NASA TR-R-11, 1959.

[10]Chapman, D. R., "An Analysis of the Corridor and Guidance Requirements for Supercircular Entry into Planetary Atmospheres," NASA TR-R-55, 1960.

[11]Marvin, J. G., and Deiwert, G. S., "Convective Heat Transfer in Planetary Gases," NASA TR-R-224, July 1965.
[12]Tauber, M. E., "A Review of High-Speed, Convective, Heat Transfer Computation Methods," NASA TP-2914, July 1989.
[13]Arthur, P. D., Shultz, H., and Guard, F. L., "Flat Plate Turbulent Heat Transfer at Hypervelocities," *Journal of Spacecraft and Rockets*, Vol. 3, No. 10, 1966, pp. 1549–1551.
[14]Tauber, M. E., and Sutton, K., "Stagnation Point Radiative Heating Relations for Earth and Mars Entries," *Journal of Spacecraft and Rockets*, Vol. 28, No. 1, 1991, pp. 40–42.
[15]Sutton, K., "Air Radiation Revisited," reprinted from Thermal Design of Aeroassisted Orbital Transfer Vehicles, Vol. 96, *Progress in Astronautics and Aeronautics Series*, 1985.
[16]Palmer, G., "An Efficient Explicit Thermochemical Nonequilibrium Algorithm Applied to Flows Over the AFE," AIAA Paper 89-1701, Buffalo, NY, June 1989.
[17]Malik, M. R., "Prediction and Control of Transition in Supersonic and Hypersonic Boundary Layers," *AIAA Journal*, Vol. 27, No. 11, 1989, pp. 1487–1493.
[18]Batt, R. G., and Legner, H. H., "A Review of Roughness Induced Nosetip Transition," AIAA Paper 81-1223, Palo Alto, CA, June 1981.
[19]Wilkins, M. E., and Tauber, M. E., "Boundary-Layer Transition on Ablating Cones at Speeds up to 7 km/s," *AIAA Journal*, Vol. 4, No. 8, 1966, pp. 1344–1348.
[20]Kaattari, G. E., "Effects of Mass Addition on Blunt-Body Boundary-Layer Transition and Heat Transfer," NASA TP-1139, 1978.